

Supplementary Materials

Table S1. Decomposition reaction that may occur in the course SCS synthesis with $\text{Mn}(\text{NO}_3)_2$ and various fuels. .

Component	Reactions	Conditions	Heat effect (kJ/mol)	Reference
Mn(II) nitrate, $\text{Mn}(\text{NO}_3)_2$	$\text{Mn}(\text{NO}_3)_2 \rightarrow [\text{MnONO}_3] + \text{NO}_2 \rightarrow \text{MnO}_2 + 2\text{NO}_2$	ca.240 °C	155 ± 12	[1,2]
	$\text{MnO}_2 \rightarrow \text{Mn}_2\text{O}_3$	560-570 °C	≈ 24	
	$\text{Mn}_2\text{O}_3 \rightarrow \text{Mn}_3\text{O}_4$	above 800 °C	/	
Glycine, $\text{C}_2\text{H}_5\text{NO}_2$	$4\text{C}_2\text{H}_5\text{NO}_2 + 9\text{O}_2 \rightarrow 5\text{H}_2\text{O} + 4\text{CO}_2 + \text{N}_2$	210 °C	-972.98 ± 0.12	[3]
	$4\text{C}_2\text{H}_5\text{NO}_2 \rightarrow 6\text{H}_2\text{O} + 2\text{NH}_3 + 6\text{C} + 2\text{HNCO}$	250 °C, no O_2	-528	[4]

Table S2. Overview of studies of SCS synthesis of Mn oxides.

Precursor	Fuel	Product	Conditions	Reference
$\text{Mn}(\text{NO}_3)_2$	Glycine	$\varepsilon\text{-MnO}_2$, 23 m ² /g	Heating plate evaporation/ignition; $\varphi = 0.5$	[5]
		$\varepsilon\text{-MnO}_2$, 43 m ² /g	$\varphi = 2.0$; higher φ results in better crystallinity	
$\text{Mn}(\text{NO}_3)_2$	Glyoxalic acid	$\text{Mn}_3\text{O}_4 + \text{Mn}_2\text{O}_3$, 43 m ² /g	Oven heating up to 120 °C (1h ramp, 1h hold), then annealing at 350 °C for 4h	[6]
	Ketoglutaric acid	$\text{Mn}_2\text{O}_3 + \text{Mn}_3\text{O}_4$, 23 m ² /g		
$\text{Mn}(\text{NO}_3)_2$	Glycine	Mn_2O_3 ; 43 m ² /g, 21 ± 4 nm	Oven heating at 600 °C for 20 min; $\varphi = 0.5$	[7]
		Mn_3O_4 ; 46 m ² /g, 17 ± 3 nm	500 °C, 30 min; $\varphi = 2$	
		$\text{Mn}_2\text{O}_3 + \text{MnO}_2$; 47 m ² /g	350 °C, 120 min, $\varphi = 2$	
$\text{Mn}(\text{NO}_3)_2$	Glycine	Mn_3O_4 ; 32 m ² /g	Slow evaporation in air, then heating plate ignition at 350 °C + x% of Vulcan	[8,9]
		$\text{Mn}_3\text{O}_4/\text{C}$; 5-35 nm		
MnAc_2	Ethanol	Mn_3O_4 (85%) + MnO (15%)	Flame ignition of ethanol	[10]
$\text{Mn}(\text{NO}_3)_2$	Citric acid	MnO_2 , 6.3 m ² /g	Oven evaporation at 150 °C for 5h, then annealing at 400 °C for 3h in air; $\varphi = 0$	[11]
		$\text{Mn}_3\text{O}_4 + \text{Mn}_2\text{O}_3$, 15.3 m ² /g	$\varphi = 0.5$	
		Mn_3O_4 , 31.7 m ² /g	$\varphi = 1$	
		Mn_2O_3 , 55.1 m ² /g	$\varphi = 2$	
	Urea	$\text{Mn}_3\text{O}_4 + \text{Mn}_2\text{O}_3$, 38.2 m ² /g	$\varphi = 4$	
$\text{Mn}(\text{NO}_3)_2$	Urea	68% MnO_2 + 32% Mn_2O_3 , 7.5 m ² /g	330°C evaporation/ignition in oven	[12]
		32% MnO_2 + 68% Mn_2O_3	$\varphi = 0.2$	
		22% MnO_2 + 78% Mn_2O_3	$\varphi = 0.3$	
		Mn_2O_3 , 68 ± 12 nm	$\varphi = 0.4$	
	Glycine	65% Mn_3O_4 + 35% MnO	$\varphi = 1$	
		Mn_2O_3	$\varphi = 2$	
		Mn_2O_3	$\varphi = 0.2$	
		Mn_2O_3	$\varphi = 0.3$	

References:

1. De Bruijn, T.J.W.; De Ruiter, G.M.J.; De Jong, W.A.; Van Den Berg, P.J. Thermal Decomposition of Aqueous Manganese Nitrate Solutions and Anhydrous Manganese Nitrate. Part 2. Heats of Reaction. *Thermochim. Acta* **1981**, *45*, 279–292. [https://doi.org/10.1016/0040-6031\(81\)85088-5](https://doi.org/10.1016/0040-6031(81)85088-5).
2. Nohman, A.K.H.; Ismail, H.M.; Hussein, G.A.M. Thermal and Chemical Events in the Decomposition Course of Manganese Compounds. *J. Anal. Appl. Pyrolysis* **1995**, *34*, 265–278. [https://doi.org/10.1016/0165-2370\(95\)00896-M](https://doi.org/10.1016/0165-2370(95)00896-M).
3. Yablokov, V.Ya.; Smel'tsova, I.L.; Zelyaev, I.A.; Mitrofanova, S.V. Studies of the Rates of Thermal Decomposition of Glycine, Alanine, and Serine. *Russ. J. Gen. Chem.* **2009**, *79*, 1704–1706. <https://doi.org/10.1134/S1070363209080209>.
4. Weiss, I.M.; Muth, C.; Drumm, R.; Kirchner, H.O.K. Thermal Decomposition of the Amino Acids Glycine, Cysteine, Aspartic Acid, Asparagine, Glutamic Acid, Glutamine, Arginine and Histidine. *BMC Biophys.* **2018**, *11*, 2. <https://doi.org/10.1186/s13628-018-0042-4>.
5. Yu, P.; Zhang, X.; Chen, Y.; Ma, Y. Solution-Combustion Synthesis of ϵ -MnO₂ for Supercapacitors. *Mater. Lett.* **2010**, *64*, 61–64. <https://doi.org/10.1016/j.matlet.2009.10.007>.
6. Puértolas, B.; Smith, A.; Vázquez, I.; Dejoz, A.; Moragues, A.; Garcia, T.; Solsona, B. The Different Catalytic Behaviour in the Propane Total Oxidation of Cobalt and Manganese Oxides Prepared by a Wet Combustion Procedure. *Chem. Eng. J.* **2013**, *229*, 547–558. <https://doi.org/10.1016/j.cej.2013.06.041>.
7. Piumetti, M.; Fino, D.; Russo, N. Mesoporous Manganese Oxides Prepared by Solution Combustion Synthesis as Catalysts for the Total Oxidation of VOCs. *Appl. Catal. B: Environ.* **2015**, *163*, 277–287. <https://doi.org/10.1016/j.apcatb.2014.08.012>.
8. Kéranguéven, G.; Faye, J.; Royer, S.; Pronkin, S.N. Electrochemical Properties and Capacitance of Hausmannite Mn₃O₄—Carbon Composite Synthesized by in Situ Autocombustion Method. *Electrochim. Acta* **2016**, *222*, 755–764. <https://doi.org/10.1016/j.electacta.2016.11.032>.
9. Kéranguéven, G.; Bouillet, C.; Papaefthymiou, V.; Simonov, P.A.; Savinova, E.R. How Key Characteristics of Carbon Materials Influence the ORR Activity of LaMnO₃- and Mn₃O₄-Carbon Composites Prepared by in Situ Autocombustion Method. *Electrochim. Acta* **2020**, *353*, 136557. <https://doi.org/10.1016/j.electacta.2020.136557>.
10. Shi, J.; Sun, M.; Hu, H. One-Step Combustion Synthesis of C-Mn₃O₄/MnO Composites with High Electrochemical Performance for Supercapacitor. *Mater. Res. Express* **2018**, *6*, 035511. <https://doi.org/10.1088/2053-1591/aaf58a>.
11. Guo, H.; Zhang, Z.; Jiang, Z.; Chen, M.; Einaga, H.; Shangguan, W. Catalytic Activity of Porous Manganese Oxides for Benzene Oxidation Improved via Citric Acid Solution Combustion Synthesis. *J. Environ. Sci.* **2020**, *98*, 196–204. <https://doi.org/10.1016/j.jes.2020.06.008>.
12. Mollaei, Z.; Kermani, F.; Moosavi, F.; Kargozar, S.; Khakhi, J.V.; Mollazadeh, S. In Silico Study and Experimental Evaluation of the Solution Combustion Synthesized Manganese Oxide (MnO₂) Nanoparticles. *Ceram. Int.* **2022**, *48*, 1659–1672. <https://doi.org/10.1016/j.ceramint.2021.09.245>.

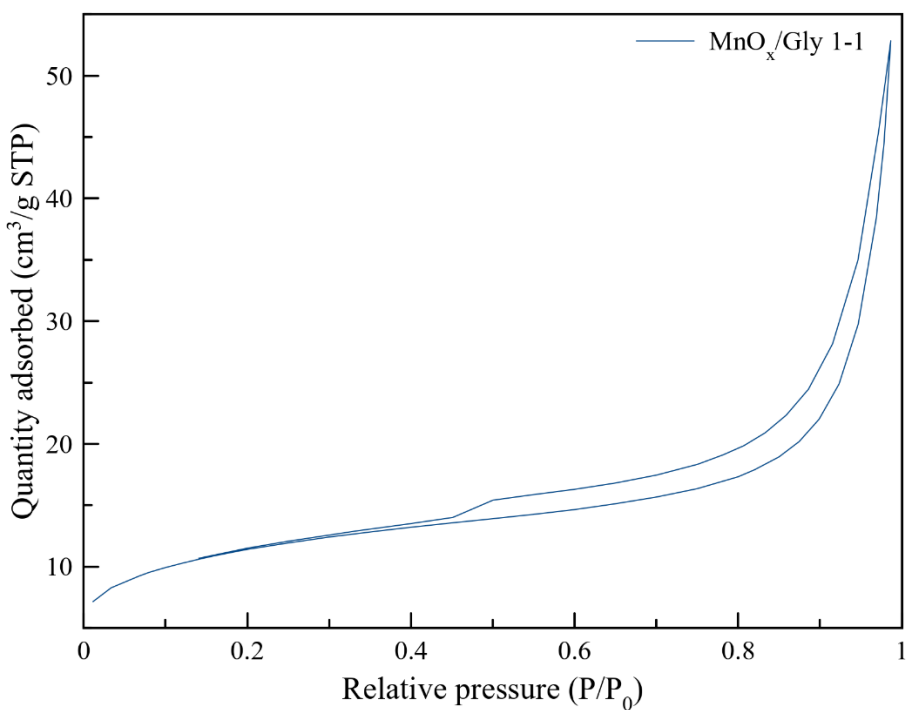


Figure S1. N_2 isotherm of the MnO_x /glycine sample.

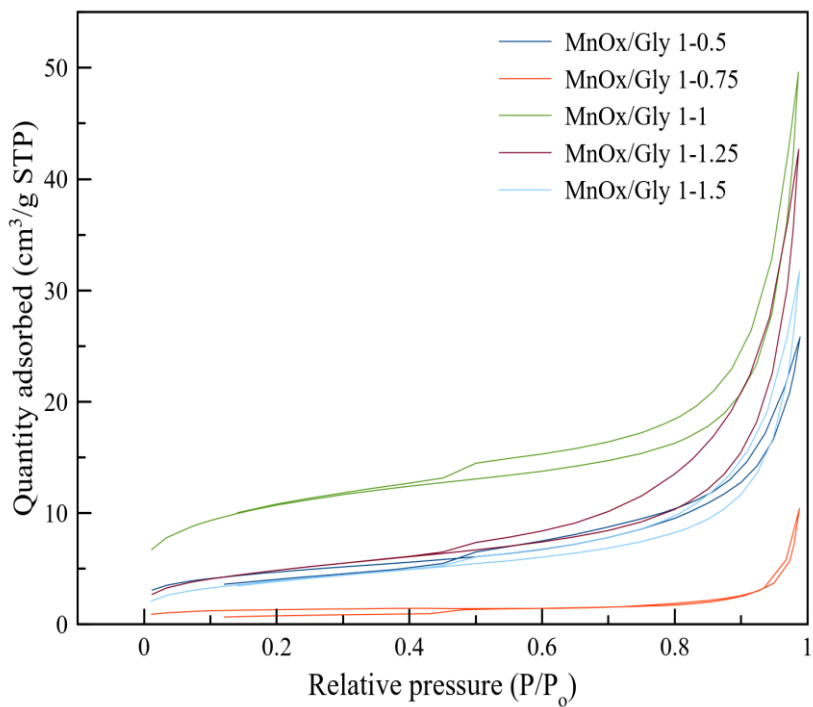


Figure S2. N_2 isotherm of the MnO_x /glycine samples with different φ ratios.

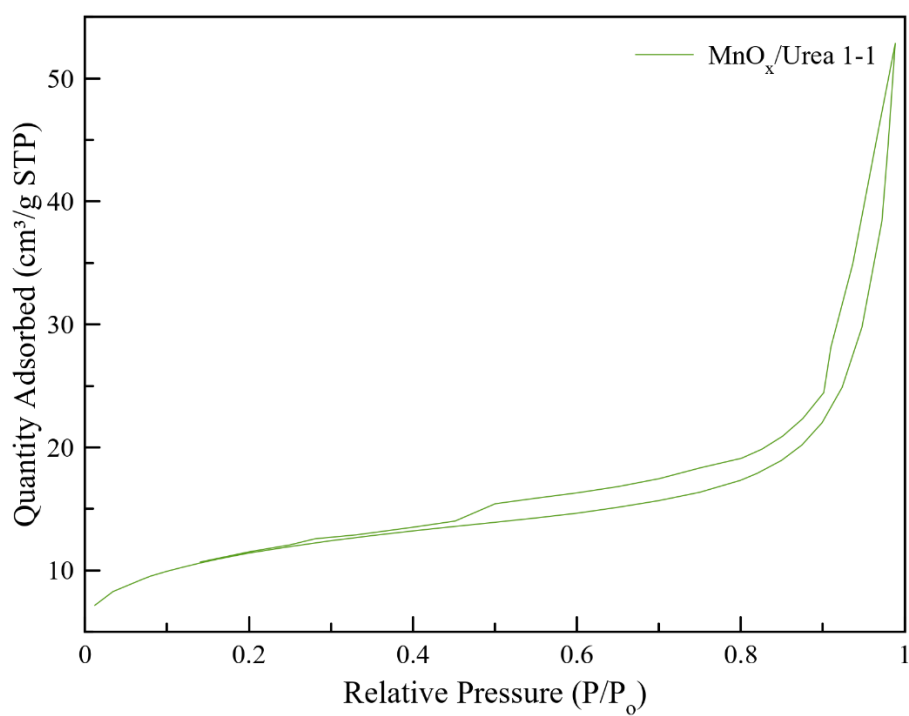


Figure S3. N_2 isotherm of the MnO_x/urea sample.

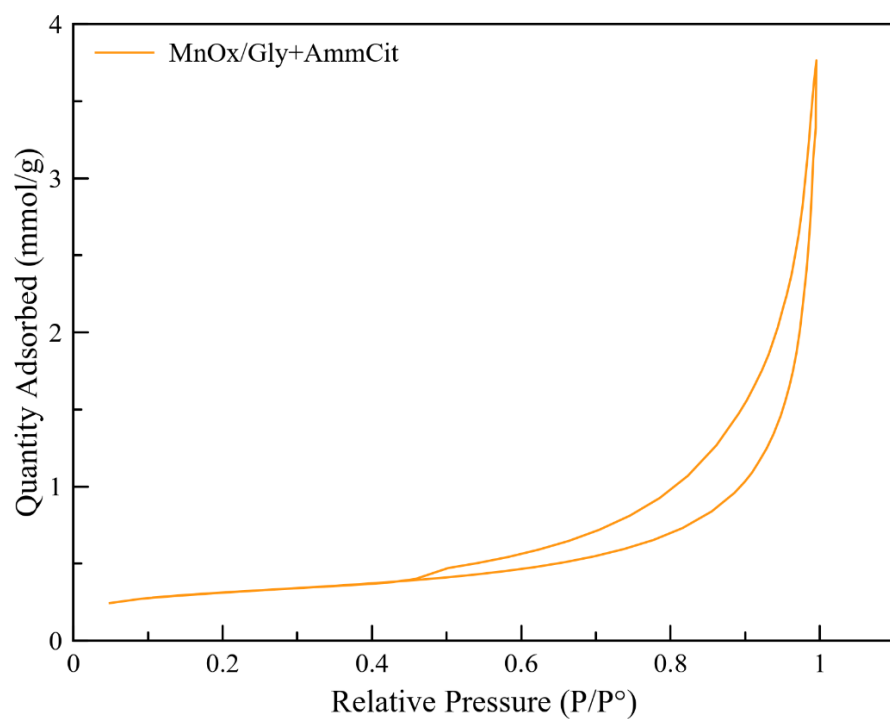


Figure S4. N_2 isotherm of the $\text{MnO}_x/\text{glycine-ammonium citrate}$ sample.

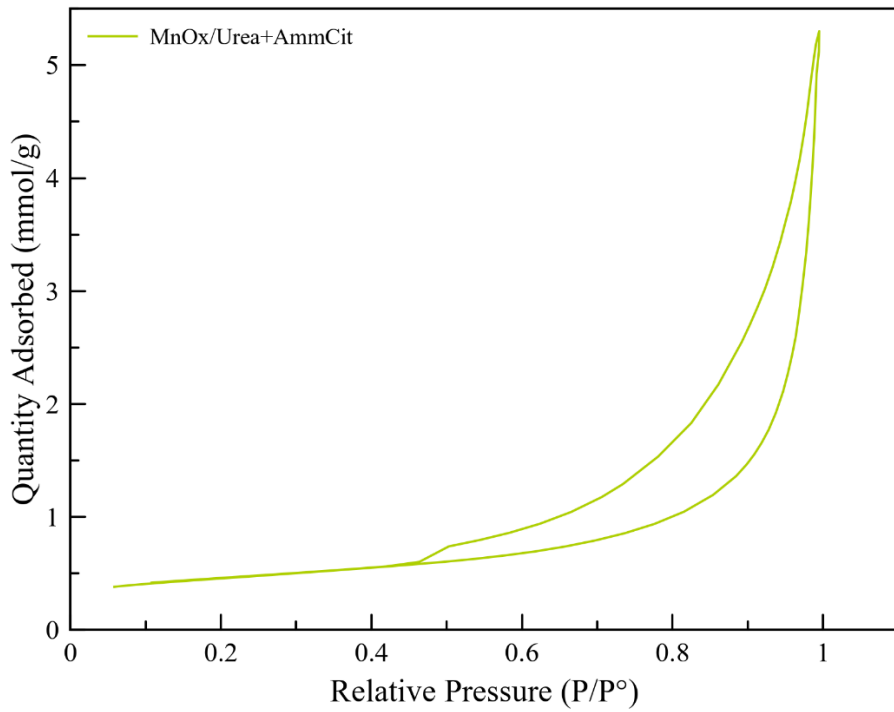


Figure S5. N₂ isotherm of the MnO_x/urea–ammonium citrate sample

The analysis of the surface-controlled and diffusion-controlled contribution to the CV currents, j , has been performed using Dunn's method. Namely, the dependence of CV currents, j , on the sweep rate, v , has been presented as:

$$j = k_1 v^{1/2} + k_2 v \quad , \quad (\text{S1})$$

where k_1 and k_2 are v -independent parameters. The first and second members of the sum correspond to diffusion-controlled and surface-controlled contributions to the current. The parameters k_1 and k_2 can be found as a slope and as intercept points of the linear dependence of j/v on $1/(\sqrt{v})$:

$$\frac{j}{v} = \frac{k_1}{v^{1/2}} + k_2 \quad . \quad (\text{S2})$$

The data for the Dunn's analysis are plotted below in Figure S6.

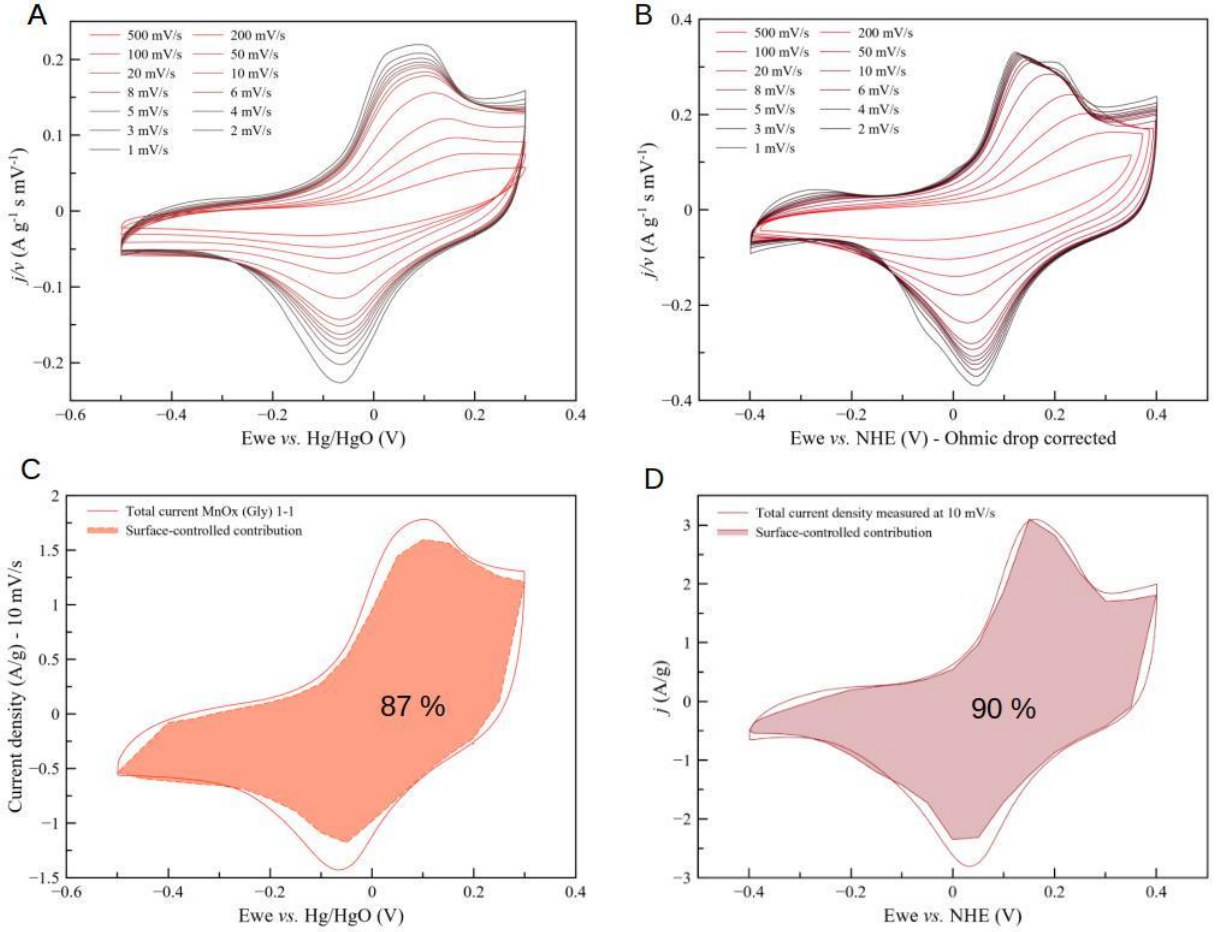


Figure S6. The CV curves for MnOx-NG (A) and MnOx-NCU (B) samples in 1 M NaOH recorded at different sweep rates. The CV curves containing only the current contribution linear to sweep rate are depicted below for MnOx-NG (C) and MnOx-NCU (D) as a filled area figure.